ADVANCED ENERGY MATERIALS
www.advenergymat.de

Efficient and Stable Blue Light Emitting Diodes Based on $CsPbBr_3$ Nanoplatelets with Surface Passivation by a Multifunctional Organic Sulfate

*He Liu, Michael Worku, Animesh Mondal, Tunde Blessed Shonde, Maya Chaaban, Azza Ben-Akacha, Sujin Lee, Fabiola Gonzalez, Oluwadara Olasupo, Xinsong Lin, J. S. Raaj Vellore Winfred, Yan Xin, Eric Lochner, and Biwu Ma**

Metal halide perovskite nanocrystals (NCs) have emerged as highly promising light emitting materials for various applications, ranging from perovskite light-emitting diodes (PeLEDs) to lasers and radiation detectors. While remarkable progress has been achieved in highly efficient and stable green, red, and infrared perovskite NCs, obtaining efficient and stable blue-emitting perovskite NCs remains a great challenge. Here, a facile synthetic approach for the preparation of blue emitting $CsPbBr_3$ nanoplatelets (NPLs) with treatment by an organic sulfate is reported, 2,2-(ethylenedioxy) bis(ethylammonium) sulfate ($EDBESO_4$), which exhibit remarkably enhanced photoluminescence quantum efficiency (PLQE) and stability as compared to pristine $CsPbBr_3$ NPLs coated with oleylamines. The PLQE is improved from ≈28% for pristine $CsPbBr_3$ NPLs to 85% for $EDBESO_4$ treated $CsPbBr_3$ NPLs. Detailed structural characterizations reveal that $EDBESO_4$ treatment leads to surface passivation of $CsPbBr_3$ NPLs by both $EDBE^{2+}$ and SO_4^{2-} ions, which helps to prevent the coalescence of NPLs and suppress the degradation of NPLs. A simple proof-of-concept device with emission peaked at 462 nm exhibits an external quantum efficiency of 1.77% with a luminance of 691 cd m^{-2} and a half-lifetime of 20 min, which represents one of the brightest pure blue PeLEDs based on NPLs reported to date.

1. Introduction

Metal halide perovskites are an emerging class of solution processable semiconductor materials with applications in various optoelectronic devices, including solar cells, LEDs, lasers, etc.[1] Thanks to the development of efficient perovskite emitters and appropriate device engineering, remarkable progress has been achieved in PeLEDs with their external quantum efficiencies (EQEs) approaching those of organic LEDs and inorganic quantum dot LEDs.[2] Despite the significant advances of PeLEDs during the last few years, many issues and challenges remain to be addressed before their commercialization, including stability, lead toxicity, and reliable processing.[3] Moreover, unlike green, red, and infrared PeLEDs exhibiting internal quantum efficiencies close to the theoretical limits,[4] the performance of blue PeLEDs with peak emissions in the region of 450–480 nm still lags behind.[5] In addition to relatively low EQEs, spectral and operational stabilities are common issues for blue PeLEDs.[6]

To achieve high-performance blue PeLEDs, highly efficient and stable blue perovskite emitters are needed, but not trivial to make. In general, due to the relatively large bandgap of blue emitters, charge-carriers could be easily captured by interband traps, resulting in high nonradiative recombination rate and low PLQEs.[7] To obtain blue perovskite emitters, compositional engineering and controlling the size of NCs are two main strategies of color tuning well explored to date.[8] Among all blue emitting perovskites, mixed halide perovskites (such as $CsPbBr_xCl_{3-x}$) are relatively easy to prepare, but often suffer from lattice mismatch and phase segregation with low stability, especially under external forces, such as photoexcitation and the presence of an electric field.[9] Quantum-confined $CsPbBr_3$ NCs and NPLs have recently been successfully developed as highly efficient blue emitters with PLQEs up to near-unity in solution.[10] However, translating them into highly efficient and stable thin films, and subsequently high-performance PeLEDs, has been less successful due to several challenges.[11] For blue emitting $CsPbBr_3$ NPLs, the formation of quantum confined 2D

H. Liu, A. Mondal, T. B. Shonde, M. Chaaban, A. Ben-Akacha, S. Lee, F. Gonzalez, O. Olasupo, X. Lin, J. S. R. Vellore Winfred, B. Ma
Department of Chemistry and Biochemistry
Florida State University
Tallahassee, FL 32306, USA
E-mail: bma@fsu.edu
M. Worku, B. Ma
Materials Science and Engineering Program
Florida State University
Tallahassee, FL 32306, USA
Y. Xin
Magnet Science and Technology
National High Magnetic Field Laboratory
Tallahassee, FL 32310, USA
E. Lochner
Department of Physics
Florida State University
Tallahassee, FL 32306, USA
The ORCID identification number(s) for the author(s) of this article can be found under https://doi.org/10.1002/aenm.202201605.

DOI: 10.1002/aenm.202201605

structure is believed to be a result of the competition between Cs^+ and protonated organic ligands during the crystal growth in solution.[12] The weak interactions between organic ligands and perovskite surfaces often lead to surface vacancy defects and coalescence of NPLs with poor photophysical properties, when NPLs in solution are processed to form thin films.[13] Also, long chain organic ligands commonly used for surface passivation are insulators which are not desirable for device applications.[14] Recently, short organic and inorganic ligands with strong binding affinity have been developed for surface passivation of blue-emitting $CsPbBr_3$ with enhanced spectral and thermal stability, which have led to blue PeLEDs with moderate efficiency and stability.[15]

Here we report a facile synthetic approach for the preparation of surface passivated $CsPbBr_3$ NPLs, by introducing an organic sulfate, 2,2-(ethylenedioxy) bis(ethylammonium) sulfate ($EDBESO_4$), into $CsPbBr_3$ NPL precursors. Our hypothesis is that $EDBESO_4$ could interact with $CsPbBr_3$ through both $EDBE^{2+}$ and SO_4^{2-} to occupy Cs vacancies and bind uncoordinated lead atoms on the surface. The $EDBESO_4$ treated $CsPbBr_3$ NPLs are found to exhibit significantly improved PLQE and stability as compared to pristine $CsPbBr_3$ NPLs with capping ligands of oleylamine and oleic acid, which could be translated into thin films with little-to-no coalescence. In addition, the replacement of long ligands with shorter $EDBESO_4$ promote charge carrier transport and enable efficient LEDs. With $EDBESO_4$ treated $CsPbBr_3$ NPLs as emitter, spectrally stable blue PeLEDs with an emission peak at 462 nm have been fabricated to exhibit EQEs of up to 1.77% and luminance of 691 cd m^{-2}.

2. Results and Discussion

2.1. Structure and Morphology of Pristine and $EDBESO_4$ Treated $CsPbBr_3$ NPLs

Colloidal $EDBESO_4$ treated $CsPbBr_3$ NPLs were synthesized by using a modified heat-up method.[15b,16] The detailed synthetic procedures could be found in the supporting information (Figure S1, Supporting Information). Briefly, $EDBESO_4$ was introduced into a precursor solution containing cesium-oleate and lead bromide during the growth of NPLs. The structural and morphological properties of $EDBESO_4$ treated $CsPbBr_3$ NPLs were characterized by scanning transmission electron microscopy (STEM) and X-ray diffraction (XRD). STEM and XRD characterizations were consistent with the prediction that the surface passivation treatment would not affect the structural or morphological properties of NPLs. **Figure 1**a displays the dark-field STEM images of $EDBESO_4$ treated $CsPbBr_3$ NPLs. The average lateral dimensions are determined to be 6.7 ± 1 nm $\times$ 26 ± 2 nm, and a lattice spacing of 0.58 nm is indexed in the inset, corresponding to the (110) plane of orthorhombic $CsPbBr_3$ phase. The size of $EDBESO_4$ treated $CsPbBr_3$ NPLs is more uniform than that of pristine $CsPbBr_3$ NPLs (Figure S2, Supporting Information). Powder XRD was used to characterize the structures of pristine $CsPbBr_3$ and $EDBESO_4$ treated $CsPbBr_3$ NPLs (Figure 1b). These two XRD patterns are similar and agree with the orthorhombic $CsPbBr_3$ reference, suggesting that surface passivation with $EDBESO_4$ does not cause lattice distortions to $CsPbBr_3$ NPLs. To determine the interactions of SO_4^{2-} and Pb^{2+} on the surfaces of $CsPbBr_3$ NPLs, X-ray photoelectron spectroscopy (XPS) was used to analyze the element compositions of pristine and $EDBESO_4$ treated $CsPbBr_3$ NPLs, with results shown in Figure 1c. A shift of 0.3 eV for the Pb 4f binding energy from pristine $CsPbBr_3$ NPLs to $EDBESO_4$ treated $CsPbBr_3$ NPLs is likely the result of stronger bonding between Pb^{2+} and SO_4^{2-} ions. The appearance of a S 2p peak is characteristic of S^{6+} in SO_4^{2-}, which is not shown in pristine $CsPbBr_3$ NPLs (Figure 1d).

The interactions between $EDBE^{2+}$ and metal halides were characterized using Fourier transform infrared spectroscopy (FTIR). The characteristic asymmetrical stretch of C-O-C at 1123 cm^{-1} of $EDBESO_4$ shifts to a lower wavenumber of 1118 cm^{-1} for $EDBESO_4$ treated $CsPbBr_3$ NPLs, which is likely due to that lone pair electrons on the oxygen atom of C-O-C interact with Pb^{2+} through coordination bond (**Figure 2**a).[17] Interactions of the amino groups of $EDBE^{2+}$ and metal halides could not be ascertained due to the presence of residual oleylamine. Scanning electron microscopy (SEM) with elemental mapping and X-ray fluorescence (XRF) were used to confirm the interactions between Pb^{2+} and SO_4^{2-} on the surfaces of $CsPbBr_3$ NPLs via the presence of sulfur signals. An elemental mapping in Figure S3, Supporting Information shows the presence of S and O along with Cs, Pb, and Br, all with a mostly uniform spatial distribution in a densely packed film of $EDBESO_4$ treated $CsPbBr_3$ NPLs. The plot of XRF for S $K_{\alpha 1}$ and S $K_{\beta 1}$, as well as the calibration curves are shown in Figure 2b and Figure S4, Supporting Information. The compositions of Pb, Br, Cs, and S in these samples could be quantitively determined according to the XRF results, which are comparable to theoretical values obtained from their chemical formulas (Table S1, Supporting Information). For pristine $CsPbBr_3$ NPLs containing three layers of metal halides, the theoretical ratio of Cs: Pb: Br = 0.76: 1: 3.33 is determined according to their formula of $L_2[CsPbBr_3]_2PbBr_4$, where L is a monovalent organic ligand. A similar ratio of Cs: Pb: Br = 0.61: 1: 3.79 was obtained by analyzing the XRF results. For $EDBESO_4$ treated $CsPbBr_3$ NPLs, the signal of sulfur was detected and the ratio of Cs: Pb: Br: S was determined to be 0.35: 1: 4.39: 0.3. The Cs: Pb molar ratio decreases from 0.61:1 to 0.35:1, because Pb^{2+} ions on the NPL surfaces were partially passivated by SO_4^{2-} ions. The Cs: Br ratio decreases from 0.16:1 to 0.07:1 is likely due to that Br^- ions could bind to one of the two terminal amino groups in $EDBE^{2+}$ when $EDBESO_4$ dissociates to $EDBE^{2+}$ and SO_4^{2-} ions. In other words, $EDBESO_4$ introduces more Br^- ions into NPLs as compared to oleylamine. It was previously reported that the high concentration of Br^- in the NPLs system is beneficial for enhancing the PLQE of NPLs by eliminating the halide vacancies.[10a]

2.2. Photophysical Characteristics of Pristine and $EDBESO_4$ Treated $CsPbBr_3$ NPLs

The optical properties of pristine $CsPbBr_3$ and $EDBESO_4$ treated $CsPbBr_3$ NPLs were systematically characterized under various conditions using UV-Vis absorption spectroscopy, as well as

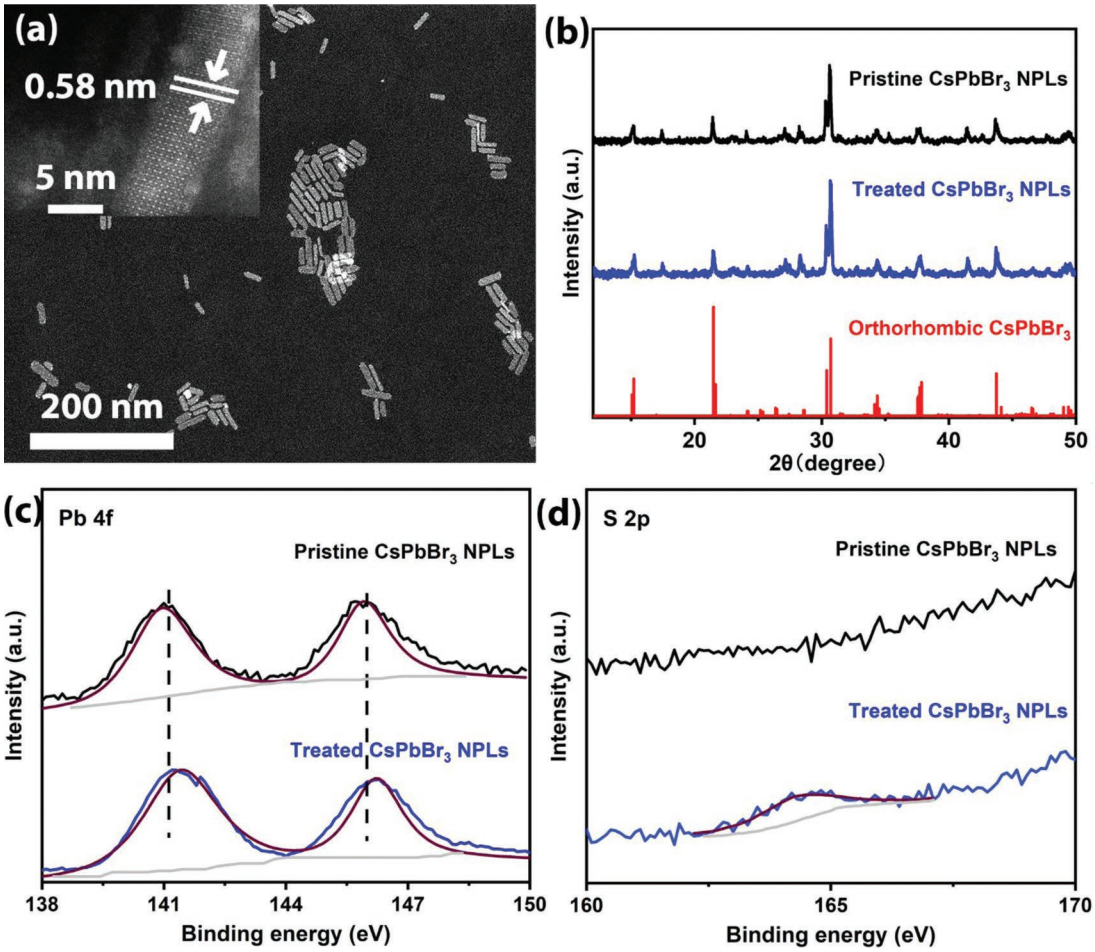

Figure 1. a) Dark-field STEM of $EDBESO_4$ treated $CsPbBr_3$ NPLs with top insert showing one NPL at higher magnification; b) powder XRD patterns of pristine $CsPbBr_3$ NPLs and $EDBESO_4$ treated $CsPbBr_3$ NPLs. The reference of orthorhombic $CsPbBr_3$ is PDF Card No. 01-085-6500; XPS spectra of c) Pb 4f and d) S 2p for thin films based on pristine $CsPbBr_3$ and $EDBESO_4$ treated $CsPbBr_3$ NPLs.

steady state and time-resolved PL spectroscopies. Figure 2c shows the absorption and emission spectra of pristine $CsPbBr_3$ NPLs and $EDBESO_4$ treated $CsPbBr_3$ NPLs in thin films. The emission of $EDBESO_4$ treated $CsPbBr_3$ NPLs peaked at 462 nm has a full width at half maximum (FWHM) of 13 nm, which is much narrower than that of pristine $CsPbBr_3$ NPLs with an FWHM of 19 nm. This suggests that $EDBESO_4$ treatment can help to achieve uniform NPLs by effectively preventing $CsPbBr_3$ NPLs from regrowing (Figure S2, Supporting Information). The PLQE of $EDBESO_4$ treated $CsPbBr_3$ NPLs in hexane solution was measured to be ≈85%, significantly higher than that of pristine $CsPbBr_3$ NPLs at 28%. The decay lifetimes were measured for both samples, with an average lifetime of 4.50 ns for $EDBESO_4$ treated $CsPbBr_3$ NPLs and 1.68 ns for pristine $CsPbBr_3$ NPLs in hexane solution (Figure 2d). The fitted parameters for PL decay curves are extracted and shown in Table S2, Supporting Information. The low PLQE of pristine $CsPbBr_3$ NPLs is not surprising, as the dissociation of highly dynamic oleylamine ligands could result in the formation of enormous halide vacancies in solution.[18] With $EDBESO_4$ treatment, surface defects are significantly reduced to suppress the nonradiative decay. Remarkably, the high performance of $EDBESO_4$ treated $CsPbBr_3$ NPLs in solution could be translated to thin films. A PLQE of 75% was recorded for neat films of $EDBESO_4$ treated $CsPbBr_3$ NPLs prepared by simple spin casting, which is more than five times higher than that of neat films based on pristine $CsPbBr_3$ NPLs (14%). These results suggest that $EDBESO_4$ treatment could effectively prevent the aggregation of NPLs and formation of defects during the formation of thin films via solution processing. The Urbach energy, which characterizes the disorder of a material via UV-vis absorption spectroscopy, was also determined for each sample from the inverse slope of $\ln \alpha$ versus energy ($h\nu$) plot. The relatively low Urbach energy (17 meV) for $EDBESO_4$ treated $CsPbBr_3$ NPLs as compared to that of pristine $CsPbBr_3$ NPLs (37 meV) strongly supports that the $EDBESO_4$ treatment helps the formation of uniform NPLs (**Figure 3**a). The increased PLQE, reduced FWHM, increased decay lifetime, and lowered Urbach energy clearly show the superior properties of $EDBESO_4$ treated $CsPbBr_3$ NPLs.

Transient absorption (TA) spectroscopy was used to further exam the exciton dynamics of these samples. As shown in Figure 3c, the spectra of thin films based on pristine $CsPbBr_3$ NPLs initially exhibit two bleach peaks at 460 and

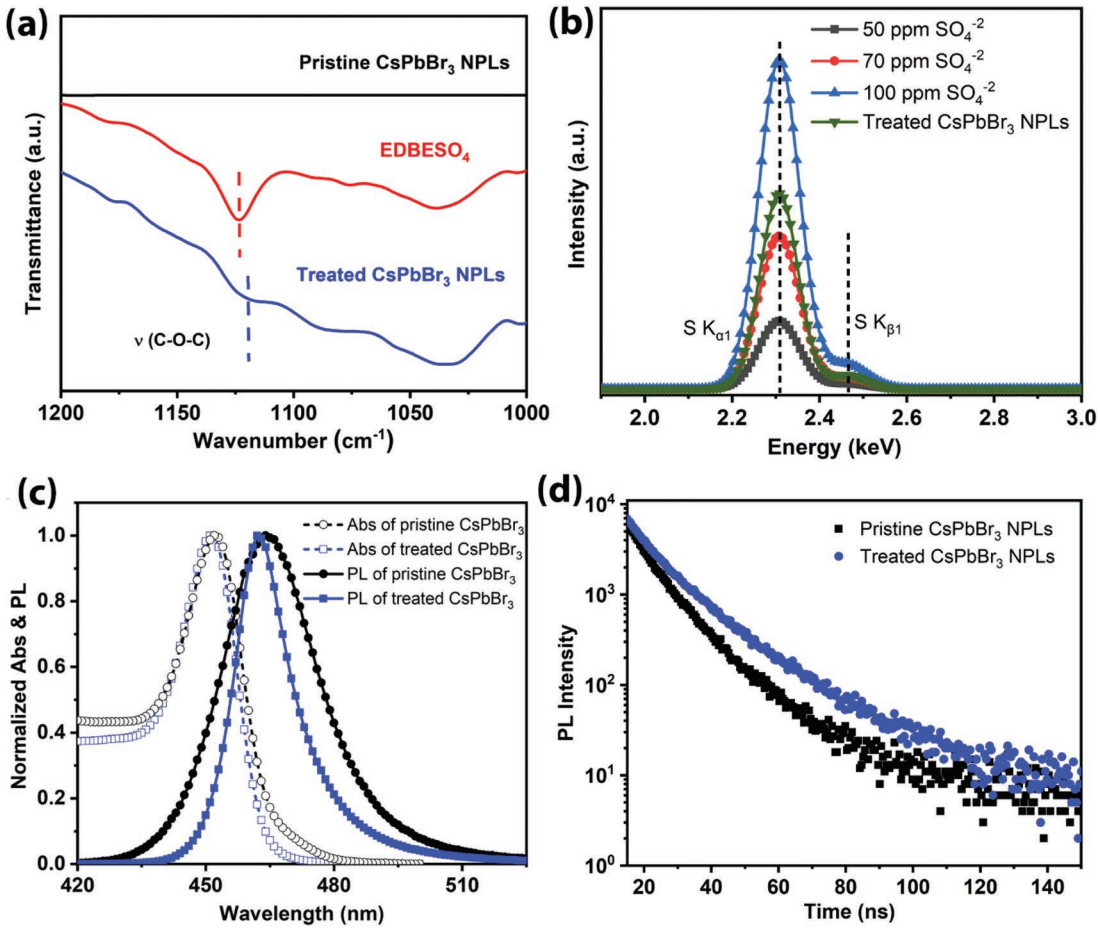

Figure 2. a) FTIR spectra of pristine $CsPbBr_3$, $EDBESO_4$, and $EDBESO_4$ treated $CsPbBr_3$ NPLs; b) energy dispersive X-ray fluorescence spectra of S in $EDBESO_4$ treated $CsPbBr_3$ NPLs and three different concentrations of reference materials (H_2SO_4) solution; c) absorption and emission spectra of pristine $CsPbBr_3$ and $EDBESO_4$ treated $CsPbBr_3$ NPLs; d) fluorescence decay curves, PLQEs and lifetimes of pristine $CsPbBr_3$ and $EDBESO_4$ treated $CsPbBr_3$ NPLs.

510 nm, corresponding to $n = 3$ and $n > 3$ $[PbBr_6]^{4-}$ octahedra in NPLs.[19] A broad bleach signal ≈510–520 nm redshifts with the increasing of delay time, which is believed to be the result of the ultrafast energy transfer between metal halide quantum wells with different thicknesses. In contrast, TAS for thin films based on $EDBESO_4$ treated $CsPbBr_3$ NPL sexhibit a single bleach peak at 460 nm, which is narrower, more stable, and does not redshift with the increasing of delay time (Figure 3d). These results suggest that $EDBESO_4$ treated $CsPbBr_3$ NPLs are very uniform in terms of size and shape.

2.3. Stability of Pristine and $EDBESO_4$ Treated $CsPbBr_3$ NPLs

Besides PL characteristics, stability is another critical parameter for light emitting materials. As many previous studies have suggested, the instability of perovskite NPLs typically originates from the defect sites on their surfaces.[20] We have performed detailed analysis to reveal the effects of $EDBESO_4$ treatment on the improved stability of $CsPbBr_3$ NPLs under ambient conditions and against damages caused by polar solvents and UV irradiation. To elucidate how $EDBESO_4$ effectively passivates the surfaces of $CsPbBr_3$ NPLs, we designed control experiments by adding the same molar ratios of SO_4^{2-} and $EDBE^{2+}$ ions into the synthetic process using different reactants, i.e., octylammonium sulfate (OctAm-SO_4) for SO_4^{2-} and $EDBEBr_2$ for $EDBE^{2+}$. The optical properties and stability against polar solvents of products prepared using different reactants were characterized, with results shown in Figure 3b and Figure S5, Supporting Information. The sample processed with OctAm-SO_4 exhibited similar blue emission with a broader emission profile (FWHM = 45 nm) and a lower PLQE (PLQE = 30%), as compared to the sample processed with $EDBESO_4$. This is likely due to $EDBE^{2+}$ not only having two amine groups, but also two ether groups which could passivate the surface defects. For the sample processed with $EDBEBr_2$, multiple emission peaks were observed, indicating the formation of NPLs with different thicknesses. This is not surprising, as $EDBE^{2+}$ could be highly dynamical in bonding and debonding from the perovskite surfaces without passivation from SO_4^{2-}, thereby facilitating the growth of NPLs with different thicknesses.

As far as the stability against polar solvents is concerned, $EDBESO_4$ treated $CsPbBr_3$ NPLs exhibit the best stability among all the samples, with little change of PL after washing with

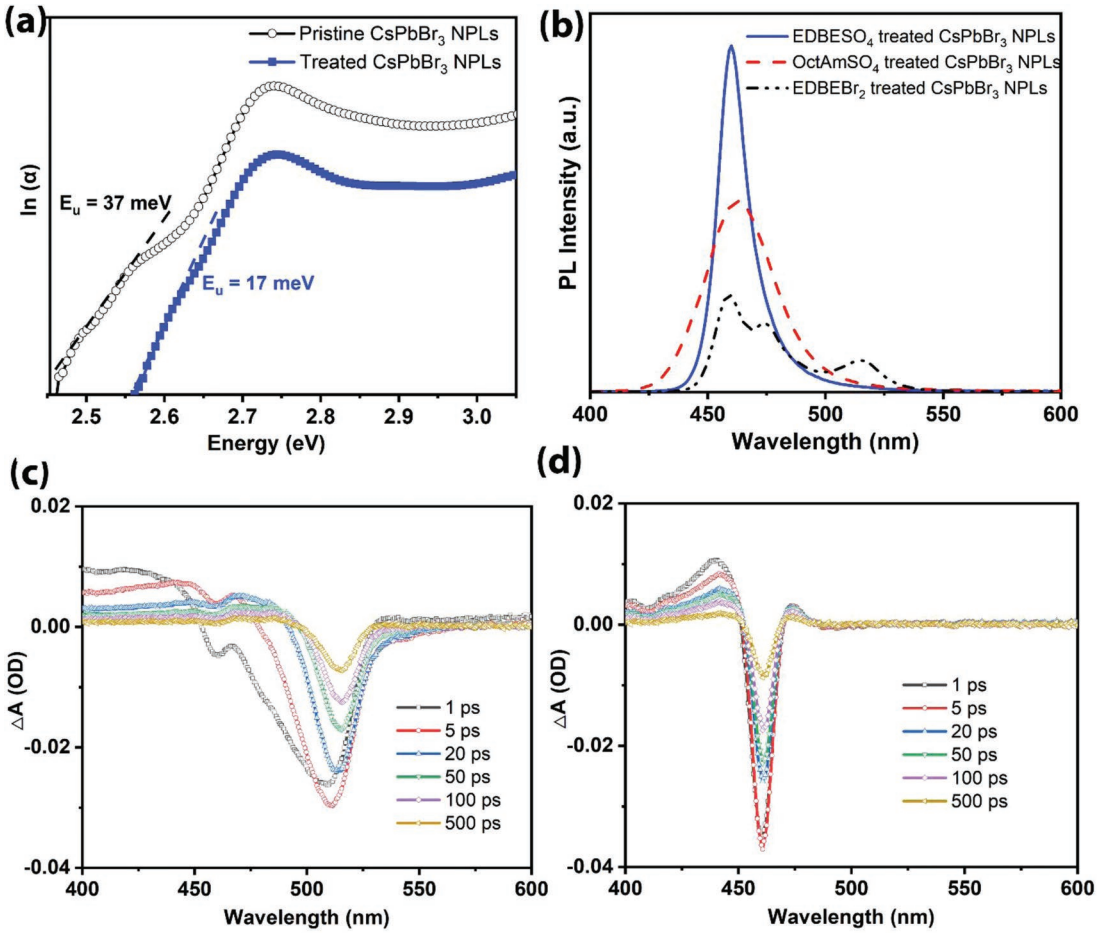

Figure 3. a) Urbach energy plots for pristine $CsPbBr_3$ NPLs and $EDBESO_4$ treated $CsPbBr_3$ NPLs in hexane solution; b) PL spectra of $CsPbBr_3$ NPLs treated with $EDBESO_4$, OctAm-SO_4, and $EDBEBr_2$; c) TA spectra of pristine $CsPbBr_3$ NPLs and d) $EDBESO_4$ treated $CsPbBr_3$ NPLs at different delay times.

methyl acetate, as shown in Figure S5, Supporting Information. TEM characterization also confirmed that the shape and size of $EDBESO_4$ treated $CsPbBr_3$ NPLs undergo almost no change after washing with methyl acetate, as shown in Figure S6, Supporting Information. In contrast, pristine $CsPbBr_3$ NPLs could barely survive the washing cycles, with a significant change of PL (Figure S5b, Supporting Information) and conversion of NPLs to cubic nanoparticles (Figure S6b, Supporting Information). The enhanced stability of $EDBESO_4$ treated samples is attributed to the multifunctionality of $EDBESO_4$, which acts as a cocktail ligand with ether, amine, and sulfate groups to passivate $[PbBr_6]^{4-}$ and decrease the abundance of vacancy defects on NPL surfaces.[21]

The stability of $EDBESO_4$ treated $CsPbBr_3$ NPLs was also evaluated in thin films. As shown in **Figure 4**a,b, the emission spectra of thin films based on $EDBESO_4$ treated $CsPbBr_3$ NPLs exhibit almost no change of peak positions with PL intensity retaining 80% of its initial value after 7 days of storage under ambient conditions, while the emission spectra of thin films based on pristine $CsPbBr_3$ NPLs clearly change with new peaks emerging within 2 days. This quick change of PL is believed to be caused by the phase transition from blue-emitting 2D NPLs to green-emitting 3D NCs for the thin films based on pristine $CsPbBr_3$ NPLs. Small angle X-ray scattering was used to characterize the structural properties and stability of these films. The self-assembly phenomenon can be detected for NPLs in thin films, as evidenced by the periodic diffraction peaks shown in Figure S7, Supporting Information. The d-spacing of 26.7 Å at $2\theta = 3.3°$ corresponds to the distance of organic ligand layers between the stacking NPLs.[10a] For fresh samples, both pristine $CsPbBr_3$ NPLs and $EDBESO_4$ treated $CsPbBr_3$ NPLs clearly show the periodic peaks, which remained for $EDBESO_4$ treated $CsPbBr_3$ NPLs after one month of storage (Figure S7a, Supporting Information), but gradually disappeared for pristine $CsPbBr_3$ NPLs after 1 day of storage (Figure S7b, Supporting Information). The photostability of thin films based on two kinds of NPLs was evaluated under continuous UV illumination (365 nm, 40 mW cm^{-2}) at ambient conditions. The blue emission of thin films based on $EDBESO_4$ treated $CsPbBr_3$ NPLs shows a slight decrease of intensity with the emission peak largely unchanged after UV illumination for 120 min (Figure 4c), whereas the emission of thin films based on pristine $CsPbBr_3$ NPLs quickly turns from blue to green in 120 min (Figure 4d).

2.4. Performance Improvement in Blue PeLEDs

The highly efficient and stable blue emission from $EDBESO_4$ treated $CsPbBr_3$ NPLs makes them of interest for use as emitter

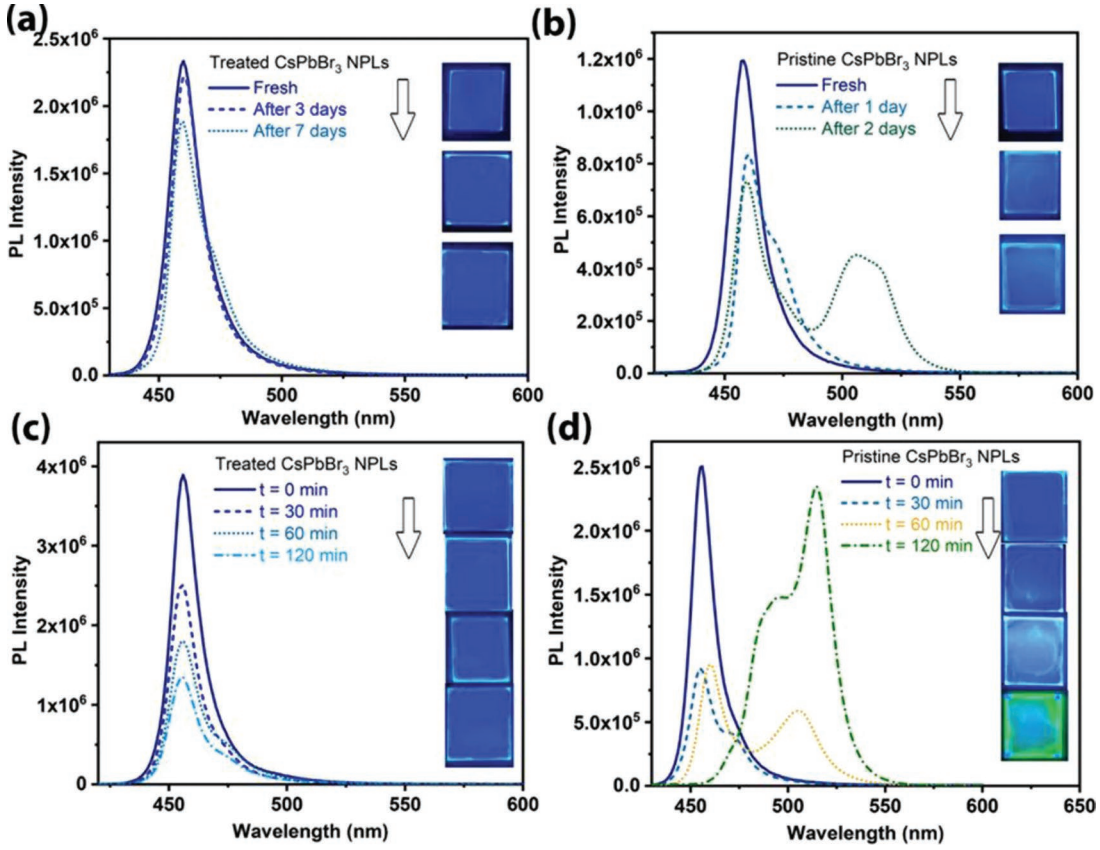

Figure 4. PL spectra of thin films with a) $EDBESO_4$ treated $CsPbBr_3$ NPLs under ambient conditions; b) pristine $CsPbBr_3$ NPLs under ambient conditions; c) $EDBESO_4$ treated $CsPbBr_3$ NPLs under continuous UV illumination; d) pristine $CsPbBr_3$ NPLs under continuous UV illumination. Corresponding inset images of thin films after detailed exposure time are shown to the right of their spectra.

in blue PeLEDs. Before device integration, smooth and uniform film morphology needs to be confirmed for thin films based on these NPLs, which is a prerequisite for high-performance LEDs. SEM and atomic force microscopy (AFM) were used to characterize solution-processed thin films based on pristine $CsPbBr_3$ NPLs and $EDBESO_4$ treated $CsPbBr_3$ NPLs. As shown in Figure S8, Supporting Information, thin films based on pristine $CsPbBr_3$ NPLs exhibit rough and uneven morphology with pin holes, which could act as electrical shunt paths affecting device efficiency. On the other hand, thin films based on $EDBESO_4$ treated $CsPbBr_3$ NPLs are smooth and uniform with a root-mean-square roughness Rq = 0.47 nm, significantly lower than that of thin films based on pristine $CsPbBr_3$ NPLs (Rq = 3.88 nm). This is not surprising, as $EDBESO_4$ treated $CsPbBr_3$ NPLs do not aggregate as much as pristine $CsPbBr_3$ NPLs in thin films.

With highly efficient, stable, and smooth blue emitting thin films based on $EDBESO_4$ treated $CsPbBr_3$ NPLs, we have fabricated LEDs using a standard device structure, ITO/PEDOT:PSS (25 nm)/poly-TPD (40 nm)/emitting layer (EML) (70 nm)/TPBi (40 nm)/LiF(1 nm)/Al (100 nm). Devices using pristine $CsPbBr_3$ NPLs as emitter were also fabricated for comparison. We carefully optimized the products by using appropriate amounts of $EDBESO_4$ during the synthesis of surface passivated $CsPbBr_3$ NPLs. A series of $EDBESO_4$ treated $CsPbBr_3$ NPLs were tested with the best results presented here. The blue emitting device based on $EDBESO_4$ treated $CsPbBr_3$ NPLs exhibited a peak EQE of 0.73% (Figure S9, Supporting Information) with a high luminance of ≈530 cd m^{-2}, significantly better than the devices based on pristine $CsPbBr_3$ NPLs. Charge imbalance in the emission layer is an important factor limiting the device efficiency of blue PeLEDs. As shown in **Figure 5**b, charge injection was quantified by measuring current density and voltage characteristics of electron-only devices (ITO/SnO_2/EML/LiF/Al) and hole-only devices (ITO/PEDOT: PSS/EML/MoO_x/Al). The results suggest that these blue PeLEDs are hole-dominant and enhancing electron injection could help to balance the charge carriers. In our study, electron transporting material TPBi was chosen to be blended into NPLs precursor solution to achieve better charge balance, with which high-performance LEDs with a maximum EQE of 1.77% and a brightness of 691 cd m^{-2} were obtained, which are among the best values reported to date for $CsPbBr_3$ based purely blue PeLEDs (Table S3, Supporting Information). As shown in Figure 5a,e, bright blue electroluminescence (EL) peak at 462 nm with CIE color coordinates of (0.136, 0.058) was recorded for the device based on $EDBESO_4$ treated $CsPbBr_3$ NPLs with TPBi doping, while a weak green emission peaked at 503 nm was recorded for the device based on pristine $CsPbBr_3$ NPLs. These results clearly suggest that pristine $CsPbBr_3$ NPLs could easily aggregate to form NCs in the presence of an electric field, while $EDBESO_4$ treated $CsPbBr_3$ NPLs with TPBi doping remained unchanged.

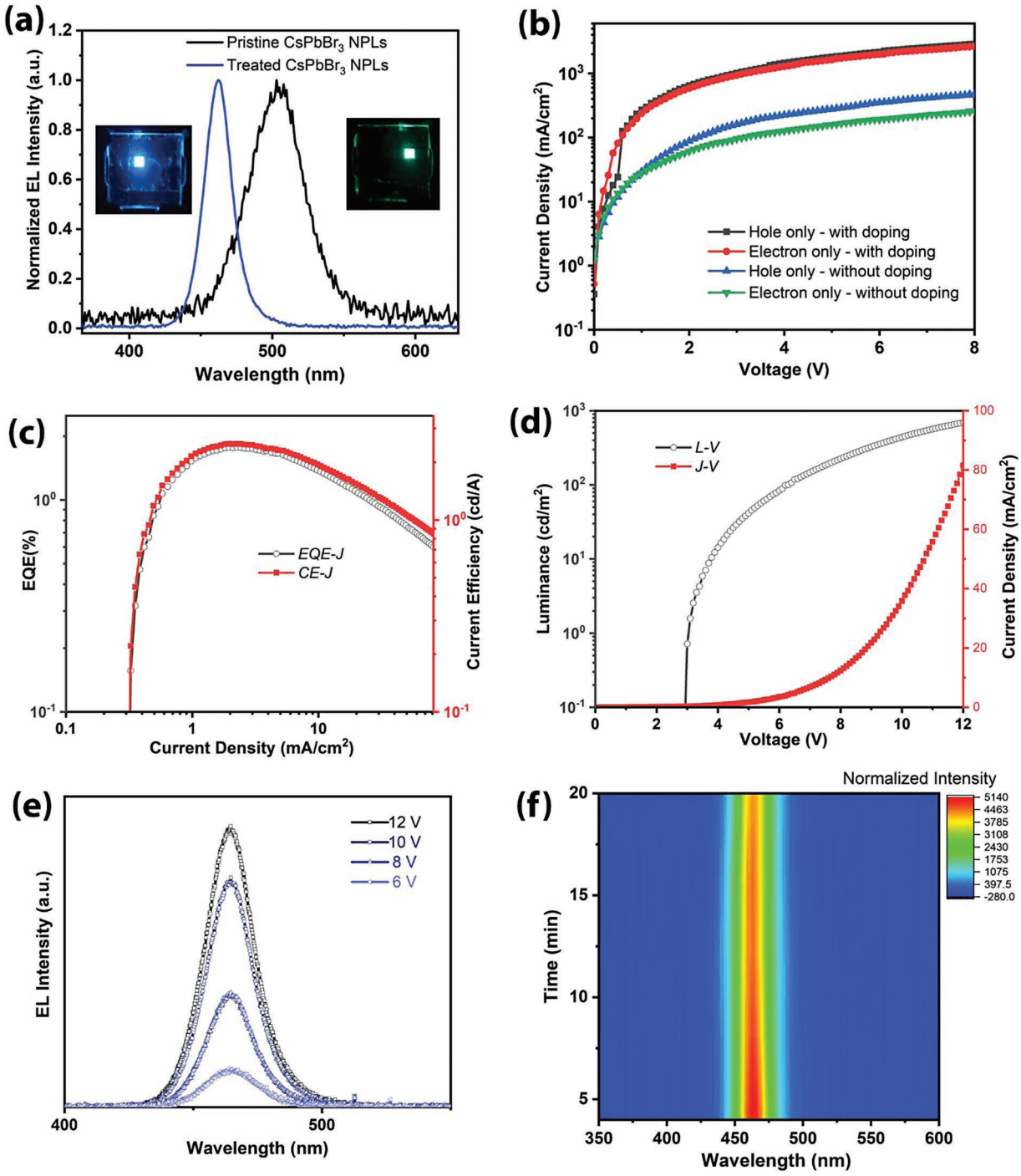

Figure 5. a) EL spectra of devices based on pristine $CsPbBr_3$ NPLs and $EDBESO_4$ treated $CsPbBr_3$ NPLs with TPBi doping; b) current density versus voltage for single carrier devices with treated $CsPbBr_3$ NPLs with and without TPBi doping; c) EQE-current density (J) -current efficiency (CE) plots for the device with treated $CsPbBr_3$ NPLs with TPBi doping; d) luminance-voltage–current density (J) plots for the device with treated $CsPbBr_3$ NPLs with TPBi doping; e) EL spectra at different bias voltages diagrams based on treated $CsPbBr_3$ NPLs device with TPBi doping; f) Change of EL spectra over the time for the device based on $EDBESO_4$ treated $CsPbBr_3$ NPLs with TPBi doping operating at 7.5 V.

The half lifetime (T50) at an initial luminance of 100 cd m^{-2} for an un-encapsulated device based on $EDBESO_4$ treated $CsPbBr_3$ NPLs doped with TPBi was measured to be ≈20 min (Figure S9d, Supporting Information), which is among the best values reported to date for blue PeLEDs with $CsPbBr_3$ as emitter.[22] The change of operation volage from 6 to 12 V does not affect the EL either, as shown in Figure 5e. Importantly, the device based on $EDBESO_4$ treated $CsPbBr_3$ NPLs exhibits remarkable spectral stability with no shift of EL after operating at 7.5 V for 20 min, as shown in Figure 5f. These results clearly

suggest that the $EDBESO_4$ treatment could effectively prevent electric field-induced phase changes, which is one of the major degradation mechanisms in PeLEDs.

3. Conclusion

In summary, we have developed a facile synthetic approach for the preparation of surface passivated $CsPbBr_3$ NPLs by using an organic sulfate ($EDBESO_4$), which exhibit a highly efficient and stable blue emission peaked at 462 nm. The cocktail surface passivation by $EDBESO_4$ is found to address many issues of blue emitting $CsPbBr_3$ NPLs for LED applications, from PLQE to film morphology and operational stability. Particularly, it prevents the second growth, aggregation, and degradation of NPLs during purification and film formation processes. With $EDBESO_4$passivated $CsPbBr_3$ NPLs as emitter, PeLEDs with a pure blue emission at 462 nm have been fabricated to exhibit remarkable spectral stability. This work clearly shows the potential of using properly surface passivated perovskite NPLs as emitter for highly efficient and stable PeLEDs.

4. Experimental Section

Chemicals: $PbBr_2$, Cs_2CO_3, 1-octadecene (90%), oleylamine (70%), oleic acid (90%), 2-propanol (IPA, anhydrous, 99.5%), octane (anhydrous, 99%), octylamine (99%), 2,2′-(Ethylenedioxy) bis(ethylamine) EDBE, 98%), H_2SO_4 (98%), poly TPD, TPBi, and LiF were purchased from Sigma–Aldrich. PEDOT:PSS (CH8000) was purchased from Heraeus.

Preparation of 2,2-(ethylenedioxy) bis(ethylammonium) sulfate ($EDBESO_4$) Ligand: $EDBESO_4$ was obtained by mixing H_2SO_4 with equivalent molar amounts of EDBE in ethanol with mild stirring in an ice water bath. The product, which was a white powder, was precipitated for 2 min and then dried under a vacuum.

Synthesis of Pristine $CsPbBr_3$ & $EDBESO_4$ Treated $CsPbBr_3$ NPLs: Pristine $CsPbBr_3$ NPLs were synthesized following previously reported procedures.[15b,16] First, cesium-oleate (CsOA) solution was prepared by dissolving 0.325 g of Cs_2CO_3 in 10 mL OA at 120°C. $PbBr_2$ solution was prepared by dissolving 0.073 g of $PbBr_2$ in 4 mL of ODE together with 0.5 mL of OLA and 0.5 ml of OA at 120 °C in a 20 mL vial. Next, 0.5 mL CsOA was added into the $PbBr_2$ solution at room temperature of 23 °C, followed by adding 0.5 mL IPA while stirring for 5 s. This was heated from room temperature (23 °C) to 70 °C at a rate of 1 °C per minute. After 10 min of heating to 70 °C, the solution was cooled using an ice water bath. The solution was centrifuged at 4000 rpm. to remove unreacted precursors. For $EDBESO_4$ treated $CsPbBr_3$ NPLs, all the other procedures were identical except for the addition of 0.01 g $EDBESO_4$ with IPA.

Purification of the Colloidal NPLs: The NPLs were collected from the 6 mL crude solution by adding 12 mL toluene (v/v ratio 1:2) and centrifuging at 4000 rpm for 5 min. Then the precipitate was purified by resuspending by shaking in 5 mL toluene and 5 mL methyl acetate solution (v/v ratio 1:1) and centrifuging and decanting the supernatant. This process was repeated once more to ensure the efficient removal of organic ligands. The NPLs were then resuspending in 2 mL of octane and used as ink solution for making the emitting layer for LED devices and material characterizations.

Fabrication of Blue LED Device: ITO glass substrates were ultrasonically washed in detergent solution, deionized water, acetone, and isopropanol for 15 min and further cleaned with a UV ozone cleaner for 20 min. PEDOT:PSS was spun-cast onto the cleaned ITO-coated glass substrate at 4500 rpm for 45 s and followed by baking at 150 °C for 20 min. Next, 8 mg ml^{-1} poly TPD solution was spin-coated at 2500 rpm for 30 s and followed by baking at 110 °C for 20 min. Then the washed NPLs ink solution was layered at 2000 rpm for 30 s. For the NPLs precursor, which was with TPBi doping, add 0.5 mL 10 mg mL^{-1} of TPBi chlorobenzene solution into the 2 mL NPLs ink solution. The thickness of the perovskite films was found to be ≈70 nm. After that, a 40 nm thick layer of TPBi and 1 nm LiF were deposited through shadow masks under a high vacuum ($<2 \times 10^{-6}$ mbar). Last, 100 nm Al was deposited as the cathode.

Characterization: Absorption spectra were taken using an Agilent Technologies Cary 5000 UV–vis–NIR spectrophotometer. The Urbach energy was calculated from the reciprocal of the slopes in the linear portion of the plot of ln (α) versus photon energy. The equation $\alpha = \alpha_0 \exp(E/E_U)$ was used with α being the absorption coefficient, α_0 being a constant, E the photon energy, and E_U being the Urbach energy. PL spectra were carried out using an Edinburgh FS5 steady-state spectrometer with a 150 W xenon lamp at an excitation wavelength of 365 nm. Time-resolved PL was collected by the same instrument. The PL decay was fit using a biexponential decay function y = A1 × exp(−x/τ1) + A2 × exp(−x/τ2) + y0, and a weighted average lifetime was calculated using $\tau ave = \Sigma \alpha i \tau i^2 / \Sigma \alpha i \tau i$, i = 1, 2, The PLQEs were acquired using a Hamamatsu Quantaurus-QY spectrometer (model C11347-11) equipped with a xenon lamp, an integrated sphere sample chamber, and a CCD detector. The PLQYs were calculated by the equation: $\eta_{QE} = I_S/(E_R\text{-}E_S)$, in which I_S represents the PL emission spectrum of the sample, E_R is the spectrum of the excitation light for the blank substrate, and E_S is the excitation spectrum for exciting the sample. The ultrafast transient absorption measurements were performed using a femtosecond (fs) pump-probe system. The output from a Ti: sapphire laser (Coherent Astrella, 100 fs, 1 kHz, 5 mJ, 800 nm), is split into two beams by a beam splitter. One beam is used to generate the pump via an optical parametric amplifier (Coherent OPerA solo). The other beam was sent to a spectrometer (Helios Fire, Ultrafast Systems LLC) to generate the probe (420–800 nm) by focussing the 800 nm fundamental onto a Sapphire crystal. Time delay between the pump and probe pulses were controlled by a motorized optical delay line. The pump beam was chopped by a mechanical chopper rotating at 500 Hz. The transient signals were recorded using a fiber-coupled CMOS detector. X-ray diffraction spectra were recorded by SmartLab X-ray diffractometer (Rigaku Corporation) with Cu Kα radiation. Scanning electron microscopy images were captured by Nova Nano SEM 400 (FEI Company) at 3.0 KV scanning voltage. XPS was conducted using a PHI 5000 series XPS equipped with a dual anode X-ray source. Al Kα radiation with a photon energy of 1486.6 eV at a take-off angle of 45° and a pass energy of 35.75 eV were used. Charge compensation was performed using adventitious C 1 s peak (284.6 eV). Spectra background was fit and subtracted using an integrated Shirley function. Dark-field STEM was acquired on a probe-aberration-corrected JEOL JEM-ARM200cF at 200 kV. AFM was taken with a Bruker Icon scanning probe microscope in tapping mode.

Device Testing: The device tests were carried out inside of a glovebox after fabrication. The electrical and optical intensity parameters of the devices were measured with a Keithly 2400 sourcemeter/multimeter coupled to an FDS 1010 Si photodiode (Thorlabs). The EL spectra of the devices were measured using an USB4000 spectrometer (Ocean Optics).

Supporting Information

Supporting Information is available from the Wiley Online Library or from the author.

Acknowledgements

The authors thank the support from the National Science Foundation (ECCS-1912911 and CHE-2005079) and the FSU Office of Research. A portion of this research used resources provided by the X-ray Crystallography Center (FSU075000XRAY) and the Materials Characterization Laboratory (FSU075000MAC) at the FSU Department of Chemistry and Biochemistry. TEM work was performed at the National High Magnetic Field Laboratory, which is supported by National Science Foundation Cooperative agreement

no. DMR-1644779 and the State of Florida. A spectrometer supported by the National Science Foundation under Grant No. CHE-1919633 was used for Transient Absorption Measurements.

Conflict of Interest

The authors declare no conflict of interest.

Data Availability Statement

The data that support the findings of this study are available from the corresponding author upon reasonable request.

Keywords

blue perovskite LEDs, $CsPbBr_3$ nanoplatelets, low dimensional perovskites, surface passivation

Received: May 11, 2022
Revised: June 22, 2022
Published online: July 22, 2022

[1] a) A. Kojima, K. Teshima, Y. Shirai, T. Miyasaka, *J. Am. Chem. Soc.* **2009**, *131*, 6050; b) Z.-K. Tan, R. S. Moghaddam, M. L. Lai, P. Docampo, R. Higler, F. Deschler, M. Price, A. Sadhanala, L. M. Pazos, D. Credgington, F. Hanusch, T. Bein, H. J. Snaith, R. H. Friend, *Nat. Nanotechnol.* **2014**, *9*, 687; c) G. Xing, N. Mathews, S. S. Lim, N. Yantara, X. Liu, D. Sabba, M. Grätzel, S. Mhaisalkar, T. C. Sum, *Nat. Mater.* **2014**, *13*, 476.

[2] a) K. Lin, J. Xing, L. N. Quan, F. P. G. de Arquer, X. Gong, J. Lu, L. Xie, W. Zhao, D. Zhang, C. Yan, W. Li, X. Liu, Y. Lu, J. Kirman, E. H. Sargent, Q. Xiong, Z. Wei, *Nature* **2018**, *562*, 245; b) L. N. Quan, B. P. Rand, R. H. Friend, S. G. Mhaisalkar, T.-W. Lee, E. H. Sargent, *Chem. Rev.* **2019**, *119*, 7444.

[3] a) M. Worku, A. Ben-Akacha, T. Blessed Shonde, H. Liu, B. Ma, *Small Sci.* **2021**, *1*, 2000072; b) L.-J. Xu, M. Worku, Q. He, B. Ma, *MRS Bull.* **2020**, *45*, 458.

[4] a) T. Chiba, Y. Hayashi, H. Ebe, K. Hoshi, J. Sato, S. Sato, Y.-J. Pu, S. Ohisa, J. Kido, *Nat. Photonics* **2018**, *12*, 681; b) Y. Cao, N. Wang, H. Tian, J. Guo, Y. Wei, H. Chen, Y. Miao, W. Zou, K. Pan, Y. He, H. Cao, Y. Ke, M. Xu, Y. Wang, M. Yang, K. Du, Z. Fu, D. Kong, D. Dai, Y. Jin, G. Li, H. Li, Q. Peng, J. Wang, W. Huang, *Nature* **2018**, *562*, 249; c) Y. H. Kim, S. Kim, A. Kakekhani, J. Park, J. Park, Y. H. Lee, H. X. Xu, S. Nagane, R. B. Wexler, D. H. Kim, S. H. Jo, L. Martinez-Sarti, P. Tan, A. Sadhanala, G. S. Park, Y. W. Kim, B. Hu, H. J. Bolink, S. Yoo, R. H. Friend, A. M. Rappe, T. W. Lee, *Nat. Photonics* **2021**, *15*, 148.

[5] a) X. Zheng, S. Yuan, J. Liu, J. Yin, F. Yuan, W.-S. Shen, K. Yao, M. Wei, C. Zhou, K. Song, B.-B. Zhang, Y. Lin, M. N. Hedhili, N. Wehbe, Y. Han, H.-T. Sun, Z.-H. Lu, T. D. Anthopoulos, O. F. Mohammed, E. H. Sargent, L.-S. Liao, O. M. Bakr, *ACS Energy Lett.* **2020**, *5*, 793; b) Q. Wang, X. Wang, Z. Yang, N. Zhou, Y. Deng, J. Zhao, X. Xiao, P. Rudd, A. Moran, Y. Yan, J. Huang, *Nat. Commun.* **2019**, *10*, 5633; c) M. Karlsson, Z. Yi, S. Reichert, X. Luo, W. Lin, Z. Zhang, C. Bao, R. Zhang, S. Bai, G. Zheng, P. Teng, L. Duan, Y. Lu, K. Zheng, T. Pullerits, C. Deibel, W. Xu, R. Friend, F. Gao, *Nat. Commun.* **2021**, *12*, 361.

[6] a) Z. Ren, K. Wang, X. W. Sun, W. C. H. Choy, *Adv. Funct. Mater.* **2021**, *31*, 2100516; b) N. K. Kumawat, X.-K. Liu, D. Kabra, F. Gao, *Nanoscale* **2019**, *11*, 2109.

[7] a) V. K. Ravi, G. B. Markad, A. Nag, *ACS Energy Lett.* **2016**, *1*, 665; b) D. P. Nenon, K. Pressler, J. Kang, B. A. Koscher, J. H. Olshansky, W. T. Osowiecki, M. A. Koc, L.-W. Wang, A. P. Alivisatos, *J. Am. Chem. Soc.* **2018**, *140*, 17760; c) C. M. Sutter-Fella, D. W. Miller, Q. P. Ngo, E. T. Roe, F. M. Toma, I. D. Sharp, M. C. Lonergan, A. Javey, *ACS Energy Lett.* **2017**, *2*, 709.

[8] a) C. Zhou, H. Lin, Q. He, L. Xu, M. Worku, M. Chaaban, S. Lee, X. Shi, M.-H. Du, B. Ma, *Mater. Sci. Eng., R* **2019**, *137*, 38; b) Y. M. Xie, Q. F. Xue, H. L. Yip, *Adv. Energy Mater.* **2021**, *11*, 2100784; c) Z. Yuan, Y. Shu, Y. Xin, B. Ma, *Chem. Commun.* **2016**, *52*, 3887.

[9] A. J. Knight, L. M. Herz, *Energy Environ. Sci.* **2020**, *13*, 2024.

[10] a) Y. Wu, C. Wei, X. Li, Y. Li, S. Qiu, W. Shen, B. Cai, Z. Sun, D. Yang, Z. Deng, H. Zeng, *ACS Energy Lett.* **2018**, *3*, 2030; b) C. Bi, Z. Yao, X. Sun, X. Wei, J. Wang, J. Tian, *Adv. Mater.* **2021**, *33*, 2006722.

[11] C. Bi, S. Wang, S. V. Kershaw, K. Zheng, T. Pullerits, S. Gaponenko, J. Tian, A. L. Rogach, *Adv. Sci.* **2019**, *6*, 1900462.

[12] a) J. Shamsi, A. S. Urban, M. Imran, L. De Trizio, L. Manna, *Chem. Rev.* **2019**, *119*, 3296; b) V. M. Burlakov, Y. Hassan, M. Danaie, H. J. Snaith, A. Goriely, *J. Phys. Chem. Lett.* **2020**, *11*, 6535; c) Y. Bekenstein, B. A. Koscher, S. W. Eaton, P. Yang, A. P. Alivisatos, *J. Am. Chem. Soc.* **2015**, *137*, 16008; d) B. J. Bohn, Y. Tong, M. Gramlich, M. L. Lai, M. Döblinger, K. Wang, R. L. Z. Hoye, P. Müller-Buschbaum, S. D. Stranks, A. S. Urban, L. Polavarapu, J. Feldmann, *Nano Lett.* **2018**, *18*, 5231.

[13] a) J. Song, T. Fang, J. Li, L. Xu, F. Zhang, B. Han, Q. Shan, H. Zeng, *Adv. Mater.* **2018**, *30*, 1805409; b) B.-B. Zhang, S. Yuan, J.-P. Ma, Y. Zhou, J. Hou, X. Chen, W. Zheng, H. Shen, X.-C. Wang, B. Sun, O. M. Bakr, L.-S. Liao, H.-T. Sun, *J. Am. Chem. Soc.* **2019**, *141*, 15423; c) Z. Dang, B. Dhanabalan, A. Castelli, R. Dhall, K. C. Bustillo, D. Marchelli, D. Spirito, U. Petralanda, J. Shamsi, L. Manna, R. Krahne, M. P. Arciniegas, *Nano Lett.* **2020**, *20*, 1808.

[14] a) E. T. Vickers, T. A. Graham, A. H. Chowdhury, B. Bahrami, B. W. Dreskin, S. Lindley, S. B. Naghadeh, Q. Qiao, J. Z. Zhang, *ACS Energy Lett.* **2018**, *3*, 2931; b) A. Heuer-Jungemann, N. Feliu, I. Bakaimi, M. Hamaly, A. Alkilany, I. Chakraborty, A. Masood, M. F. Casula, A. Kostopoulou, E. Oh, K. Susumu, M. H. Stewart, I. L. Medintz, E. Stratakis, W. J. Parak, A. G. Kanaras, *Chem. Rev.* **2019**, *119*, 4819.

[15] a) F. Yang, H. Chen, R. Zhang, X. Liu, W. Zhang, J. Zhang, F. Gao, L. Wang, *Adv. Funct. Mater.* **2020**, *30*, 1908760; b) J. Shamsi, D. Kubicki, M. Anaya, Y. Liu, K. Ji, K. Frohna, C. P. Grey, R. H. Friend, S. D. Stranks, *ACS Energy Lett.* **2020**, *5*, 1900; c) W. Yin, M. Li, W. Dong, Z. Luo, Y. Li, J. Qian, J. Zhang, W. Zhang, Y. Zhang, S. V. Kershaw, X. Zhang, W. Zheng, A. L. Rogach, *ACS Energy Lett.* **2021**, *6*, 477.

[16] J. Shamsi, P. Rastogi, V. Caligiuri, A. L. Abdelhady, D. Spirito, L. Manna, R. Krahne, *ACS Nano* **2017**, *11*, 10206.

[17] Z. Zhu, Y. Wu, Y. Shen, J. Tan, D. Shen, M.-F. Lo, M. Li, Y. Yuan, J.-X. Tang, W. Zhang, S.-W. Tsang, Z. Guan, C.-S. Lee, *Chem. Mater.* **2021**, *33*, 4154.

[18] J. T. DuBose, P. V. Kamat, *J. Phys. Chem. C* **2020**, *124*, 12990.

[19] Y. K. Wang, D. Ma, F. Yuan, K. Singh, J. M. Pina, A. Johnston, Y. Dong, C. Zhou, B. Chen, B. Sun, H. Ebe, J. Fan, M. J. Sun, Y. Gao, Z. H. Lu, O. Voznyy, L. S. Liao, E. H. Sargent, *Nat. Commun.* **2020**, *11*, 3674.

[20] S. K. Ha, C. M. Mauck, W. A. Tisdale, *Chem. Mater.* **2019**, *31*, 2486.

[21] Z. Zhu, Y. Wu, Y. Shen, J. Tan, D. Shen, M.-F. Lo, M. Li, Y. Yuan, J.-X. Tang, W. Zhang, S.-W. Tsang, Z. Guan, C.-S. Lee, *Chem. Mater.* **2021**, *33*, 4154.

[22] a) R. L. Z. Hoye, M.-L. Lai, M. Anaya, Y. Tong, K. Gałkowski, T. Doherty, W. Li, T. N. Huq, S. Mackowski, L. Polavarapu, J. Feldmann, J. L. MacManus-Driscoll, R. H. Friend, A. S. Urban, S. D. Stranks, *ACS Energy Lett.* **2019**, *4*, 1181; b) C. Zhang, Q. Wan, B. Wang, W. Zheng, M. Liu, Q. Zhang, L. Kong, L. Li, *J. Phys. Chem. C* **2019**, *123*, 26161.